

eRD12 Progress Report - Status Update on Polarimeter, Luminosity Monitor and Low Q^2 -Tagger for Electron Beam (June 2016)

June 15, 2016

Project ID: eRD12

Project Name: Electron polarimetry, low Q^2 -tagger, luminosity monitor R&D

Period Reported: from January 2016 to June 2016

Project Leader: Elke Aschenauer

Contact Person: Elke Aschenauer, Richard Petti

Project members: BNL physics: Elke-Caroline Aschenauer, Alexander Kiselev, Richard Petti, William Schmidke; BNL-CAD: Vladimir Litvinenko, Christoph Montag, Robert Palmer, Vadim Ptitsyn, Dejan Trbojevic; BNL-Magnet Division: Brett Parker

Abstract

This document describes the progress made since the last January 2016 report [9] on the eRD12 research project on the development of an electron beam polarimeter, luminosity monitor and low Q^2 -tagger projects and the general integration within the interaction region (IR). This represents the last report on the project scope and seeks to finish up remaining loose ends on the electron polarimeter design (including some analysis on the requirements for a laser system and a fitting procedure to extract the beam polarization), low Q^2 -tagger (considerations to backgrounds to physics analyses), luminosity monitor (update on how polarized cross-section can affect the measurement) and roman pot studies (acceptance and the progress of the general interaction region design with the machine developers).

1 Past

The main goal for this period of review has been to continue the development of the electron polarimetry scheme at eRHIC and make the plan more crisp. The planned activities include the further development of the transverse polarization measurement scheme, integrating the extraction of the longitudinal and transverse polarization into one detector, pursue studies related to the choice of laser system and laser requirements, continue to optimize the detector configuration in the tunnel, look into higher order corrections for the QED calculation of Compton scattering and consider the details to the polarimetry system in the two eRHIC machine design options of the ring-ring and linac-ring designs. Although not stated explicitly, tying up loose ends related to the other systems in the project (low Q^2 -tagger) and the roman pot systems were also pursued and is discussed later in this document.

The elements that still have not been completed include optimization of the polarimeter detector configuration in the tunnel and a full calculation of the spin dependent cross-section for the Bethe-Heitler process used for the luminosity measurement [8]. Considering the former case of the placement of the polarimetry system in the machine, a reasonable place has been found (see [9]), but due to a lack of detailed lattice design and beam optics parameters from the machine design group, the details of the study can only go so far. Some simple assumptions have been made to offer guidance into what may work, but in the end, the machine group needs to dedicate manpower to this effort to make significantly more progress. The latter case of the spin dependent calculation of the elastic e+p scattering is not complete, but we have begun communications with some theorists to calculate this and have already received some quantitative guidance (see section 1.5).

The remaining points of work that have been completed will be discussed in the following subsections.

1.1 Electron Beam Polarimetry Progress

The progress on the electron beam polarimetry studies are discussed in this section. Each element of the study is discussed in its own subsection below.

1.1.1 Laser Requirements and Impact to Polarization Uncertainty

One of the items that received attention in this period of review are the laser requirements for the polarimeter system. As a reminder, the electron polarimetry is based on Compton scattering of circularly polarized laser photons interacting with the electron beam, where the interaction cross-section is polarization dependent. The polarization state of the laser would be alternately flipped and the resulting asymmetry of detected photons is measured, which is a reflection of asymmetry in the interaction cross-section between the two helicity states (aligned spin versus anti-aligned spin) which is dependent on the polarization of the beam. The cross-section asymmetry is accurately calculable analytically and known

(since it is pure QED) and the beam polarization acts as a dilution factor to the measured asymmetry compared to the physical asymmetry. Thus the beam polarization can be extracted by fitting the measured photon asymmetry with the known asymmetry, with the beam polarization as a free fitting parameter (please see the references for details [9]).

Additionally, it is required to monitor the polarization for each cathode from which the beam electrons originate for the linac-ring design. The plan is to have a Gatling gun with multiple cathodes as a source for the electrons and it is desirable to monitor any possible difference in the polarization of the electrons coming from each cathode separately. If an option is pursued without the Gatling gun (such as in the ring-ring design), then it is at least required to monitor the polarization bunch by bunch to monitor potential depolarizing effects due to varying beam-beam effects.

Let us consider some of the details related to the laser system that may be required. First we start by estimating the laser power that is required to make a good polarization measurement. To set the luminosity scale, we assume that we need roughly one Compton photon per beam crossing. This assumption is later investigated when we study the time required to make a good polarization measurement. Equation 1 shows how one can calculate the luminosity at the Compton IP from basic parameters about the beam and laser. The equation is for a pulsed laser system.

$$L = \frac{f_b N_e N_\gamma}{2\pi\sigma_{x\gamma}\sigma_{y\gamma}\sqrt{1 + (0.5\theta\sigma_{z\gamma}/\sigma_{y\gamma})^2}} \quad (1)$$

$$N_{Compton}[s^{-1}] = L\sigma_{Compton} \quad (2)$$

$$N_{Compton}[bunch^{-1}] = L\sigma_{Compton}/f_b \quad (3)$$

In the equation, L is the luminosity, f_b is the bunch frequency, N_e is the number of electrons in a bunch, N_γ is the number of laser photons in a pulse, $\sigma_{(x,y,z)\gamma}$ are the widths of the laser beam in the direction transverse to the beam (x and y) and the pulse length along the beam direction (z). Table 1 summarizes reasonable parameters for the calculation either taken from estimates about the eRHIC design from the machine group [3] or parameters that have been achieved at other facilities [10].

A few other key equations are shown in equations 2 and 3, which calculate the number of Compton photons produced ($N_{Compton}$) per second and per bunch crossing respectively, which is a function of the Compton interaction cross-section, $\sigma_{Compton}$. The $\sigma_{Compton}$ is approximately 400 mb (as obtained from the Monte Carlo simulation implementing the QED calculation for Compton scattering developed from the last review period) for a 20 GeV electron colliding with a 2.33 eV laser. The energy of the laser is a typical choice that other facilities have used, though this is not a hard requirement and can be investigated further.

We set the number of Compton photons produced per bunch equal to one, do a little algebra, and arrive at the relation (shown in equation 4) for the number of photons in a

Parameter	value
f_b	9.4 MHz [3]
N_e	0.07×10^{11} [3]
σ_x	400 μm [10]
σ_y	400 μm [10]
σ_z	0.4 cm [3]
σ_{Compton}	400 mb

Table 1: A summary of machine and laser parameters entering into the calculation for the required laser power. References for where the numbers were obtained are included with the values. The numbers assume the linac-ring design.

laser pulse (i.e. the laser power) needed to achieve the production of one Compton photon per bunch with a 20 GeV electron beam hit by a 2.33 eV laser.

$$N_\gamma = \frac{2\pi\sigma_{x\gamma}\sigma_{y\gamma}\sqrt{1 + (0.5\theta\sigma_{z\gamma}/\sigma_{y\gamma})^2}}{N_e\sigma_{\text{Compton}}} \quad (4)$$

Using the above equations and the values in table 1, we calculate that we need 3.6×10^{12} laser photons per bunch to achieve the production of one Compton photon per beam crossing at the beam and laser energy described above. For a 2.33 eV laser, this translates to a pulse energy of 1.3 μJ . Thus the total power of the laser required for this scenario is approximately 12 W for a laser pulsed at a frequency of 9.4 MHz, timed synchronously with the eRHIC clock. This is a very reasonable laser and can be readily obtained from various companies (for example Lumentum [1], with their industrial class of lasers which include lasers with a wavelength of 532 nm (2.33 eV), a total output power ranging from mW to 50 W and a repetition rate ranging from single shot to 400 MHz). This estimate shows that a Fabry-Perot type cavity to boost the laser power to the kW range (as is done at Hall A at JLab [10]) is likely unnecessary and thus saves a good deal of engineering.

Next we investigate the time required to make a good polarization measurement assuming cathode by cathode monitoring under the above scenario. As a reminder, the polarization of the beam can be calculated from equation 5, with the counting asymmetry (Σ) defined in equation 6 as the difference of the photon counts with interactions in each helicity state (N^+ and N^-) normalized by the total photon rate, N . The analyzing power is given by A and is determined by a convolution of the physical asymmetry and detector smearing effects. It can then be shown that the statistical uncertainty on the electron polarization, δP_e is given by equation 7.

$$P_e = \frac{\Sigma}{A} \quad (5)$$

$$\Sigma = \frac{N^+ - N^-}{N^+ + N^-} = \frac{N^+ - N^-}{N} \quad (6)$$

$$\delta P_e \approx \frac{1}{\sqrt{N}} \frac{1}{A} \quad (7)$$

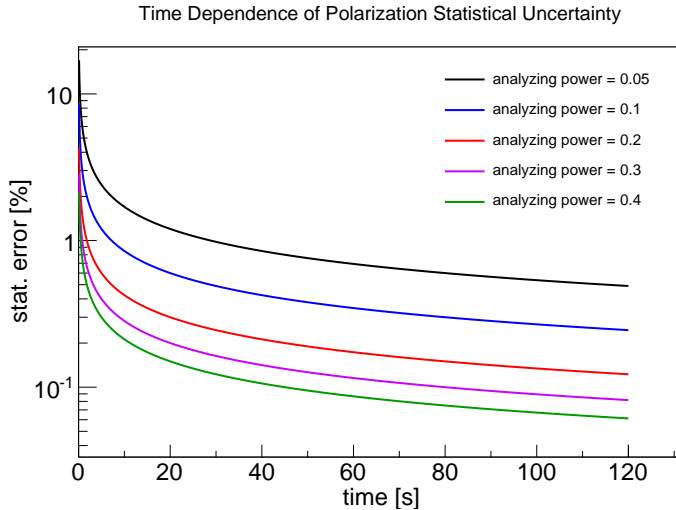


Figure 1: The measurement time dependence of the statistical uncertainty of the polarization measurement for cathode by cathode monitoring in the linac-ring design. The different colors represent the calculation assuming different analyzing powers as denoted in the legend.

Using the above equations, we correlate the amount of time needed to make a measurement with the associated statistical uncertainty. As discussed many times, it is critical to have a polarization measurement accurate to better than 1%. Since the measurement will most likely be dominated by systematic uncertainties, we also want to keep the statistical uncertainty below this cut off. Some further considerations go into calculating the time to monitor the polarization cathode by cathode. We start by considering the number of bunches. The number of bunches is planned to be the same as at RHIC, 120 bunches (for the linac-ring design option). Of these 120, only 111 are filled [3]. Further the current Gattling gun approach assumes a total of 20 cathodes [3]. Finally we assume that half of the bunches will have a specific polarization. Using this information, an effective bunch crossing rate tracking a bunch produced from a single cathode is calculated as $R = 9.4 \times 10^6 (111/120)(1/20)(1/2) = 2.2 \times 10^5$ or a little over a factor of 10 reduction in

Issue	linac-ring	ring-ring
cathode by cathode fluctuations	yes	no
beam-beam interactions	no	yes

Table 2: A table listing some of the important issues that concern the linac-ring and the ring-ring polarimetry designs.

rate compared to the true bunch frequency. We also assume peak electron polarization of the beam of 0.8 [3] to calculate the fractional statistical uncertainty. The results are shown as a function of the analyzing power and summarized in figure 1, with the different colored lines showing the calculation for different analyzing powers.

The results show that even at a poor analyzing power of 0.05 (note that the longitudinal asymmetry peaks at 0.4), it will only take about 2 minutes to get a 1% statistical uncertainty on a cathode by cathode based monitoring of the electron beam polarization. This also justifies the running of the polarization measurement in so-called single photon mode, which has benefits over running in multi-photon mode since it seems that the time required for the measurement (which is typically a drawback of single photon running) is not an issue due to the larger beam current of the eRHIC machine compared to other previously or currently running facilities.

Note that the above mentioned procedure is only valid in the linac-ring scheme as in this scheme each bunch is dumped after the collision. In the ring-ring design, where the electron beam will circulate many times, this measurement procedure would deplete the electron beam somewhat. Some of the different issues plaguing the measurement for the linac-ring vs ring-ring designs are shown in table 2.

1.1.2 New Fitting Procedure for Polarization Extraction

The progress of the polarization extraction analysis has been discussed in the last progress report. At that time, a procedure to extract the longitudinal polarization by measuring the scattered photon and the scattered electron was modeled and implemented. This was a full simulation modeling detector smearing and digitization and was proven to be successful in that we could extract from the fit the polarization that was input to the simulation. For this current period of review, we investigated schemes to extract the transverse polarization. Though this is expected to be small, it is important to be aware of this component if it exists and will also help to tune the spin rotator magnets. Previous experiments and facilities typically have separate devices to measure each polarization component, as the detector requirements are different depending on what is desired to be measured. A longitudinally polarized beam displays an asymmetry in the cross-section which is dependent only on the energy of the scattered photon. A transversely polarized beam breaks the azimuthal symmetry, and thus the cross-section asymmetry depends on the azimuthal scattering angle of the photon in addition to the energy dependence. See the previous report [9] for more

details. This means that to measure longitudinal polarization, one only needs a calorimeter with good energy resolution, where to measure transverse polarization, the calorimeter also needs to be finely segmented to observe the position asymmetry due to the azimuthal angle dependence. There is no reason a priori why these two procedures cannot be merged into a single detector. This has been investigated.

The current design of the detector implemented in the simulation consists of an electromagnetic calorimeter sitting behind a pre-shower detector. The pre-shower detector consists of three silicon tracking layers interspersed with layers of 2mm thick Tungsten, similar to the setup for the PHENIX MPC-EX [5]. The calorimeter consists of 30 mm² x 200 mm PbWO₄ towers. This allows good position resolution as well as energy resolution. A simple photon track reconstruction algorithm to determine the angle of the photon track (given the vertex position) was implemented based on the hits in the tracking layers from the particle shower. Figure 2 shows energy resolution and the angular resolution of the photons in the left and right-side plots respectively for this setup.

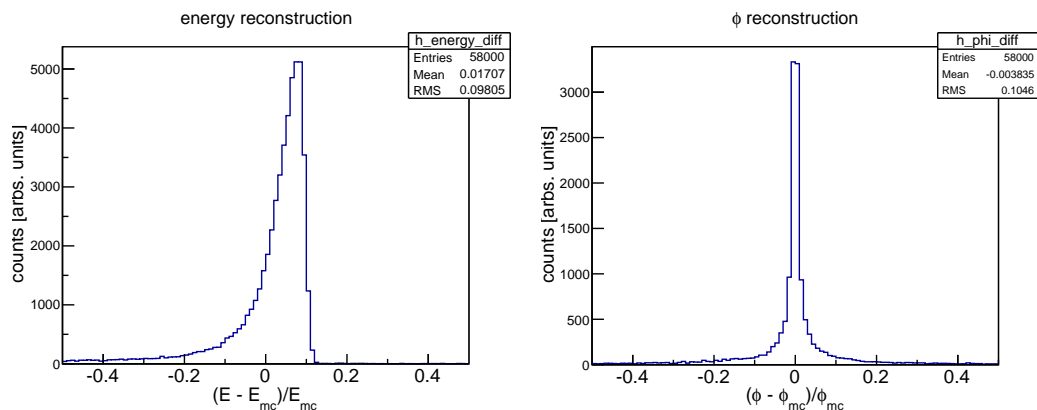


Figure 2: Evaluation of the reconstruction of the photon energy (E) and azimuthal angle (ϕ) in the current detector setup.

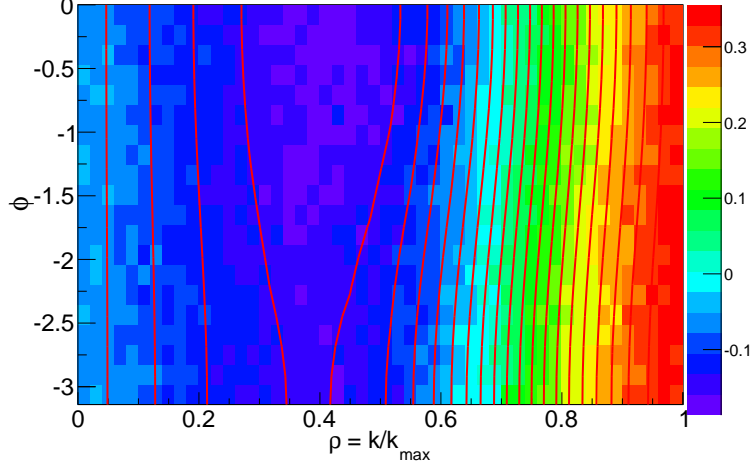


Figure 3: The asymmetry distribution of photons as a function of photon energy (ρ) and azimuthal scattering angle (ϕ). The coloring represents the strength of the asymmetry. The red contours indicate the results of the fitting procedure.

$$\frac{d^2\sigma}{d\rho d\phi} = \frac{d^2\sigma_0}{d\rho d\phi} \mp P_e P_\gamma \left(\cos\Psi \frac{d^2\sigma_1}{d\rho d\phi} + \sin\Psi \cos\phi \frac{d^2\sigma_2}{d\rho d\phi} \right) \quad (8)$$

$$\frac{d^2\sigma_0}{d\rho d\phi} = r_0^2 a \left[\frac{(\rho(1-a))^2}{1-\rho(1-a)} + 1 + \left(\frac{1-\rho(1+a)}{1-\rho(1-a)} \right)^2 \right] \quad (9)$$

$$\frac{d^2\sigma_1}{d\rho d\phi} = r_0^2 a \left[(1-\rho(1+a)) \left(1 - \frac{1}{(1-\rho(1-a))^2} \right) \right] \quad (10)$$

$$\frac{d^2\sigma_2}{d\rho d\phi} = r_0^2 a \left[\rho(1-a) \frac{\sqrt{4a\rho(1-\rho)}}{1-\rho(1-a)} \right] \quad (11)$$

$$\frac{d^2 A}{d\rho d\phi} = \left(\frac{d^2\sigma^+}{d\rho d\phi} - \frac{d^2\sigma^-}{d\rho d\phi} \right) / \left(\frac{d^2\sigma}{d\rho d\phi} \right) \quad (12)$$

$$(13)$$

For this simulation, Compton scattering events have been generated with the Monte Carlo written that draws from the analytic calculation for the polarization dependent cross-section. The photons from the scattering are then measured in the calorimeter in a full scale simulation. At this stage of the study, we only use the pure Monte Carlo information and will add in the complication of detector smearing and granularity once the procedure has been stabilized on the pure information. For this simulation, the polarization fraction

is set to 0.8 and the polarization angle of 0.11 is input to the simulation, which translates to a 10% percent transverse component. The asymmetry as a function of the polarization angle (Ψ), scattered photon energy (ρ) and azimuthal angle (ϕ) is shown in equation 12. Equal number of events with each helicity state are generated. The counting asymmetry, $((N^+ - N^-)/(N^+ + N^-))$, of the photons as a function of scattering angle and energy is shown in figure 3. A two-dimensional fit using equation 12 is done on the distribution in figure 3, which is shown by the red contour lines. A two parameters fit is used, which represent the polarization fraction and the polarization angle. If successful, this would allow simultaneous extraction of the polarization, as well as the transverse and longitudinal components. The extracted polarization and polarization angle from the fit is 0.742 ± 0.002 and 0.1202 ± 0.004 respectively. While the angle is well constrained, the polarization is underestimated by several σ of uncertainty. Improvement to the fits and other additional constraints to improve the results are still being investigated.

1.2 Progress on the Roman Pot Acceptance Studies

Significant progress has been made with respect to the interaction region designs from the machine design group. Brett Parker has designed an improved layout for the hadron beam compared to the previous version studied (proton acceptance results from previous design reported in [8], which gave a push for the new version). A first IR layout for the ring-ring design by Christoph Montag was also released. The new designs prompted the establishment of a new format for information exchange of the IR layout between the machine group and the machine users. This change has greatly increased the efficiency in information exchange and allows accelerated iteration in the designs. The EicRoot package has been modified to implement the reading in of the IR lattice from the new file format. This emphasizes that developments in this project advance developments in the Monte Carlo package to facilitate these studies, which can be of general use to the community as a whole.

Figure 4 shows a schematic of the new layouts for the newest v3.01 linac-ring (left) and v1.0 ring-ring (right) designs. As was done in the study with the previous IR layout, Deeply Virtual Compton Scattering (DVCS) events were generated by the MILOU Monte Carlo [6] for 20 GeV electrons colliding with 250 GeV protons. The particles were sent through the IR setup in EicRoot. The acceptance results are shown in figure 5 as a function of the scattered proton p_T and compares the three IR designs that we currently have (the old linac-ring (v2.1), the new linac-ring (v3.01) and the first ring-ring design). First note that the acceptance is significantly better in the new linac-ring design compared to the old design. The new design has near perfect proton acceptance and this improvement was largely pushed by the findings of the previous study. The current ring-ring design is significantly worse at high p_T to the limit of it being unacceptable to do DVCS physics. Improvement to acceptance can be as simple as increasing the aperture of the magnets, though it is still under discussion as to how much of an increase is reasonable and still

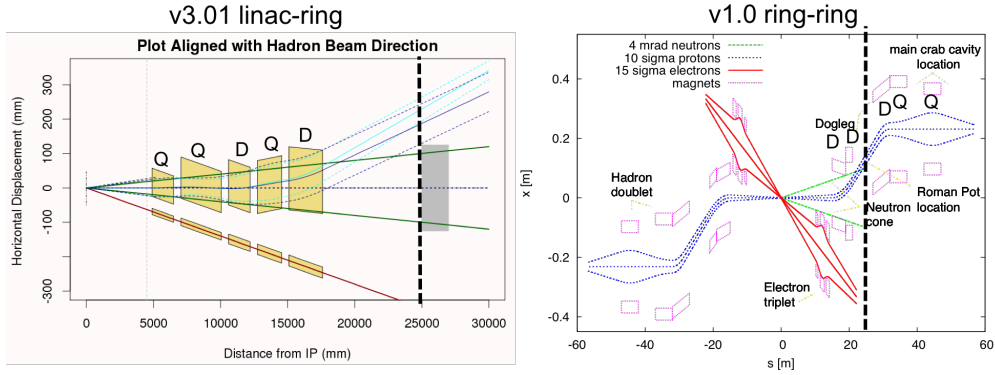


Figure 4: The newest IR layouts for the linac-ring (left) and ring-ring (right) machine designs. Magnets are denoted as a bending dipole (D) or focusing quad (Q) on the figure. The dotted line represents the location in z of the roman pot installation (25m and 28m for the linac-ring and ring-ring design respectively).

results in a magnet that can be manufactured.

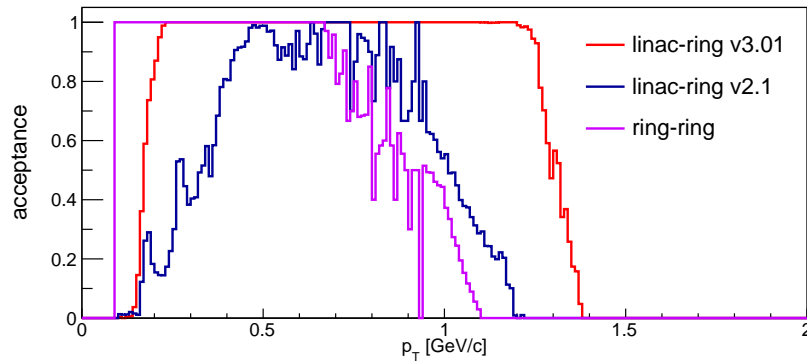


Figure 5: A comparison of the acceptance as a function of the proton p_T for the three IR designs currently developed with protons generated from MILOU simulations of DVCS events for 20 GeV electrons colliding with 250 GeV protons.

The situation is much worse for collisions with lower proton energies, as the expected distribution of the scattered protons in DVCS widens as shown in figure 6.

The importing of the magnetic fields into the simulation allows one to scale the fields to simulate running with different beam energies. Figure 7 shows the comparison of the proton acceptance for the linac-ring v3.01 design with 250 GeV and 100 GeV proton beam. The acceptance is cutoff in p_T around 0.6 GeV/c. Luckily, the distribution of the scat-

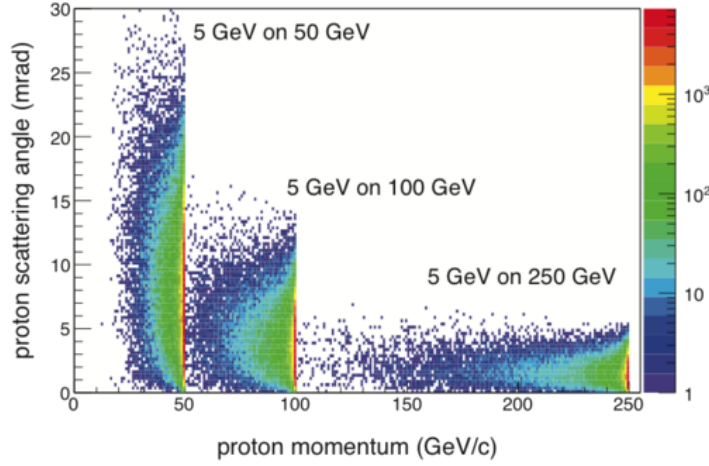


Figure 6: A comparison of the scattering angle and momentum dependence for protons from DVCS events at different proton collision energies produced by a MILOU simulation.

tered proton has little dependence on the electron energy, so we can achieve a reasonable kinematic reach by studying 250 GeV protons colliding with varied electron energies.

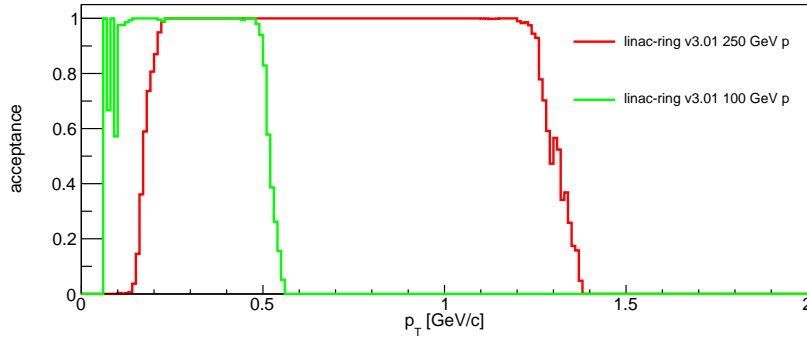


Figure 7: A comparison of the acceptance as a function of the proton p_T in the linac-ring v3.01 IR design for DVCS simulations with 250 GeV and 100 GeV proton collisions.

1.3 Verification of Neutron Acceptance

A study was done to verify that we have sufficient acceptance for neutrons from processes in which the beam ion breaks up in the reaction. J.H. Lee has done simulations using the DPMJet model [2] to determine the distribution of neutrons from the nuclear breakup in 20 GeV electrons colliding with 50 GeV, 75 GeV, and 100 GeV gold ions. The results are

shown in figure 8. Neutrons generated according to these distributions are then fed into the EicROOT framework with the corresponding IR layouts.

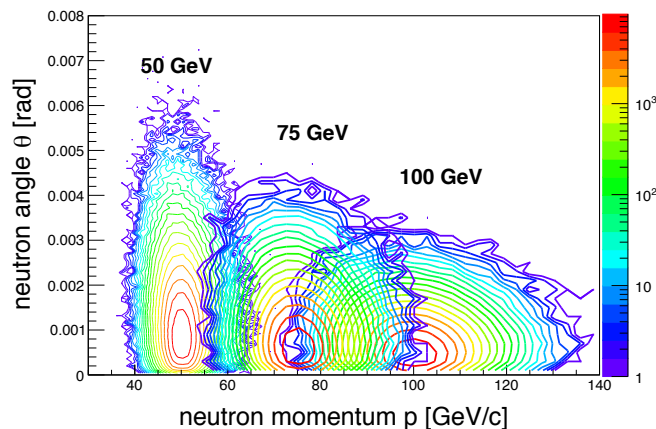


Figure 8: A plot of the expected breakup neutron distribution in relative yield, scattering angle, and momentum modeled in the DPMJet Monte Carlo code for 20 GeV electrons colliding with Au ions of various energies as depicted in the figure.

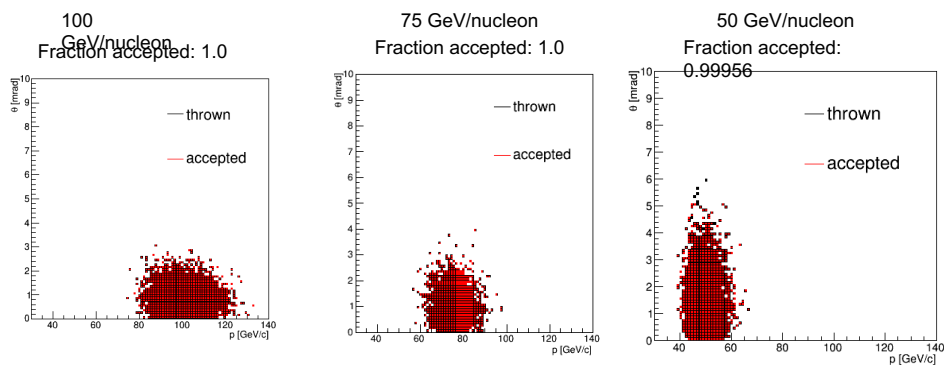


Figure 9: The acceptance of the generated neutrons from nuclear breakup in the v3.01 version of the linac-ring IR, shown for different Au beam collision energies.

Figures 9 and 10 show the results of the simulations for the latest linac-ring v3.01 configuration, as well as for the ring-ring layout. The results are good in that nearly all neutrons pass through the magnet lattice to where a ZDC may be placed for either IR design and for all ion collision energies.

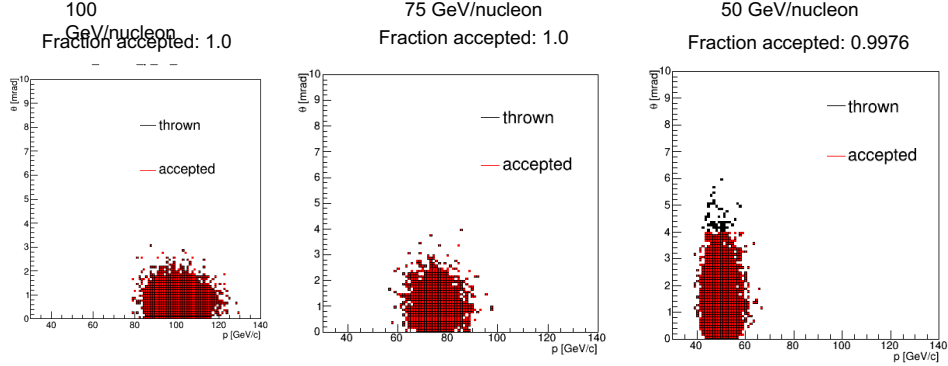


Figure 10: The acceptance of the generated neutrons from nuclear breakup in the ring-ring IR, shown for different Au beam collision energies.

1.4 Progress on the Low Q^2 -tagger Studies

An initial design, placement into the IR, and acceptance study related to a low Q^2 -tagger have been presented in previous reports [7, 8, 9], along with a simple reconstruction algorithm to determine the scattering angle of the electron (allowing the calculation of the Q^2 of the event). For this review period, we started to investigate the feasibility of using the detector for analysis in light of the large background from elastic e-p scattering (the same process that will be used for the luminosity measurement). Simulations show that many of the scattered electrons from this process will actually hit the low Q^2 -tagger, representing a significant level of background events that need to be rejected in order to isolate events with a low Q^2 . Due to the setup of the beam line (utilizing the old v2.1 linac-ring IR layout), the electrons that hit the tagger fall in a specific energy region as shown in figure 11.

We performed an estimate of the expected background rates from this process. The below calculations are considering 20 GeV on 250 GeV electron-proton collisions. First, the rate of electrons coming from interesting PYTHIA generated events is estimated. From the cross-section calculated from PYTHIA (determined to be approximately 140 nb), it is determined that electrons from these events (and assuming a machine luminosity of $4.1 \times 10^{33} \text{ cm}^{-2} \text{ s}^{-1}$) will be produced at a rate of 560 electrons per second. Conversely, the background source of electrons from the elastic e-p scattering (Bethe-Heitler process) is estimated as well. Considering an energy range of electrons from 11 to 15 GeV for the electrons that hit the tagger (see figure 11), the corresponding cross section is 24 mb, much greater than that for the interesting physics events. This represents a great background and translates to roughly ten electrons per bunch coming from the background Bethe-Heitler process and about 1×10^{-4} electrons per bunch from interesting DIS events. Keep in mind these are rough numbers and still need to account for the physical acceptance of

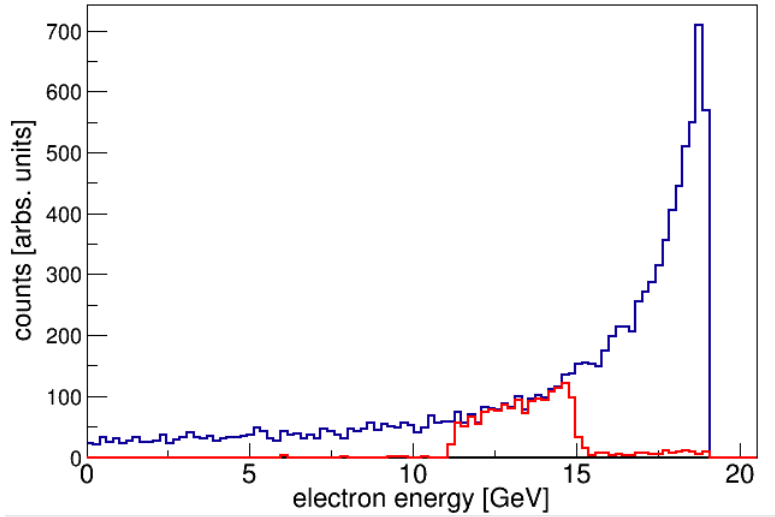


Figure 11: The energy range of background electrons that hit the low Q^2 -tagger from the Bethe-Heitler process at with 20 GeV electrons colliding with 250 GeV protons (shown in red) compared to all primary electrons emitted from the process (blue).

these electrons in the tagger from the PYTHIA events, but still gives some indication of the scale of the issue. It is possible that strategic placement of the tagger could help to alleviate this while still balancing acceptance from interesting events. This would be a natural extension of the current study.

Another avenue for investigation is quantifying the effect of rejecting events with a coincidence in the luminosity monitor and the low Q^2 -tagger with the total energy equal to the electron beam energy, indicating a Bethe-Heitler event. More simulations are needed to prove the effectiveness of this as well as to develop other methods utilizing the current design of the tagger with the tracking layers in front of the calorimeter to measure the track multiplicity in the detector.

1.5 Dependence of the Luminosity Measurement on the Beam Polarization

As discussed in previous reports [7, 8, 9], the plan for the luminosity measurement is to measure photons from the accurately known process of elastic electron-proton scattering (so-called Bethe-Heitler process after the first physicists to calculate the cross-section for the process in QED). While explicit and analytical calculations exist for the case of unpolarized beams, a similar calculation does not yet exist for polarized beams (when both the electron and the proton are polarized). This is very important, as the luminosity calculation is based on the known cross-section. One of the deliverables of this project is the

calculation of this polarization dependent cross-section. We have started to communicate with theorists who are interested in calculating the dependence. We have some guidance at the moment from Dieter Müller, who has estimated the ratio of $d\sigma^{long.pol}/d\sigma^{unpol}$ goes roughly as Q^2/s , with s the center of mass energy of the collision, which is derived from equations contained in [4]. At the large center of mass energies, this ratio is small and so deviations of the polarized cross section from the unpolarized cross section are small.

2 Future

This is the final report for the eRD12 project, as this closes the two year period of funding. The project was largely a success and helped to orient the IR designs to converge to a workable design, as well as developed the initial design for several critical detector components. For the future, the main proponents of eRD12 are submitting a proposal for an additional year of funding to pursue studies related to expected backgrounds from the machine (synchrotron radiation, beam-gas interactions, beam-beam interactions, neutron flux), which can have a great impact on the detector technologies that can be used, as well as the physics analyses that will be feasible. This proposal is submitted in a second document.

3 Manpower

Manpower working on the project is summarized below, listed in alphabetical order, but separated by department.

- Elke Aschenauer - BNL physics. Provides project guidance and is the supervisor of the project.
- Alexander Kiselev - BNL physics. Provides software support.
- Richard Petti - post-doc at BNL working under the supervision of Elke Aschenauer. Performed the bulk of the work and works on the project full time.
- William Schmidke - BNL physics. Provides project guidance through expertise in polarimetry.
- Vladimir Litvinenko - BNL-CAD. Provides project guidance through expertise on the collider side. Facilitates machine related discussions.
- Christoph Montag - BNL-CAD. Provides the magnet design for the interaction region for the ring-ring machine design.
- Robert Palmer - BNL-CAD. Provides the magnet design for the interaction region for the ring-ring machine design.

- Brett Parker - BNL-CAD/Magnet division. Provides the magnet design of the interaction region for the linac-ring machine design.
- Vadim Ptitsyn - BNL-CAD. Provides project guidance and design of the spin rotator magnets.
- Dejan Trbojevic - BNL-CAD. Provides project guidance through expertise in the machine lattice design.

4 Publications

A manuscript is in progress which will incorporate the findings of this study and elaborate on the constraints and requirements from the physics on the detectors. This will be combined with the progress of the design of a dedicated eRHIC main detector (BEAST), and is expected to be completed shortly. The target journal is NIM or JHEP.

5 Closing Remarks and Executive Summary

The initial scope of the eRD12 project has largely been completed. The fluidity of the IR design (and even the machine concept as a whole) makes constant monitoring and iteration of the study for each design and option essential in this ongoing process. The items that the project sought to achieve and have successfully done (with references indicating where this was reported) are:

- Initial design and integration into the IR of a low Q^2 -tagger for electrons scattered from low Q^2 events, along with identifying main constraints from physics [7, 8].
- Initial design and integration of the luminosity monitor into the IR and identification of main constraints due to physics [7, 8].
- Initial design and integration of the electron beam polarimeter into the machine lattice and identification of main constraints due to physics [9].
- Investigations into the forward proton acceptance and impact into measurements [7, 8, 9].

References

- [1] <https://www.lumentum.com/en/commercial-lasers/products/commercial-laser-product-finder>.
- [2] <https://wiki.bnl.gov/eic/index.php/DPMJet>.

- [3] E. C. Aschenauer et al. eRHIC Design Study: An Electron-Ion Collider at BNL. 2014.
- [4] Andrei V. Belitsky, Dieter Mueller, and A. Kirchner. Theory of deeply virtual Compton scattering on the nucleon. *Nucl. Phys.*, B629:323–392, 2002.
- [5] S. Campbell et al. A Proposal for the Muon Piston Calorimeter Extension (MPC-EX) to the PHENIX Experiment at RHIC. 2013.
- [6] E. Perez, L. Schoeffel, and L. Favart. MILOU: A Monte-Carlo for deeply virtual Compton scattering. 2004.
- [7] R. Petti et al. eRD12 Progress Report - Status Update on Polarimeter, Luminosity Monitor and Low Q²-Tagger for Electron Beam (Jan 2015), 2015. https://wiki.bnl.gov/conferences/images/2/24/ERD12_report.pdf.
- [8] R. Petti et al. eRD12 Progress Report - Status Update on Polarimeter, Luminosity Monitor and Low Q²-Tagger for Electron Beam (June 2015), 2015. https://wiki.bnl.gov/conferences/images/4/4e/ERD12_report_2015-6.pdf.
- [9] R. Petti et al. EIC Detector R&D Progress Report (Jan 2016), 2016. <https://wiki.bnl.gov/conferences/images/1/1f/Erd12-january2016.pdf>.
- [10] A. Rakhman et al. A high-finesse fabryperot cavity with a frequency-doubled green laser for precision compton polarimetry at jefferson lab. *Nucl. Instrum. Meth.*, A822:82–96, 2016.